TOPICAL REVIEW — 2D materials: physics and device applications

# Graphene resistive random memory — the promising memory device in next generation*

Xue-Feng Wang(王雪峰)[1,2], Hai-Ming Zhao(赵海明)[1,2], Yi Yang(杨轶)[1,2,†], and Tian-Ling Ren(任天令)[1,2,‡]

[1] *Institute of Microelectronics, Tsinghua University, Beijing* 100084, *China*

[2] *Tsinghua National Laboratory for Information Science and Technology (TNList), Tsinghua University, Beijing* 100084, *China*

(Received 30 August 2016; revised manuscript received 5 October 2016; published online 18 January 2017)

Graphene-based resistive random access memory (GRRAM) has grasped researchers' attention due to its merits compared with ordinary RRAM. In this paper, we briefly review different types of GRRAMs. These GRRAMs can be divided into two categories: graphene RRAM and graphene oxide (GO)/reduced graphene oxide (rGO) RRAM. Using graphene as the electrode, GRRAM can own many good characteristics, such as low power consumption, higher density, transparency, SET voltage modulation, high uniformity, and so on. Graphene flakes sandwiched between two dielectric layers can lower the SET voltage and achieve multilevel switching. Moreover, the GRRAM with rGO and GO as the dielectric or electrode can be simply fabricated. Flexible and high performance RRAM and GO film can be modified by adding other materials layer or making a composite with polymer, nanoparticle, and 2D materials to further improve the performance. Above all, GRRAM shows huge potential to become the next generation memory.

**Keywords:** graphene-based resistive random access memory, graphene oxide (GO)/reduced graphene oxide (rGO), resistive switching, graphene

**PACS:** 85.25.Hv, 68.65.Pq, 88.30.mj, 72.80.Vp **DOI:** 10.1088/1674-1056/26/3/038501

## 1. Introduction

Resistive random access memory (RRAM) is a kind of memory based on a resistive switching mechanism controlled by external voltage.[1–6] Its simple metal-insulating layer-metal structure can break through technological and physical limitations existing in ordinary memory devices such as dynamic random access memory (DRAM) and flash as the device scales down and has higher storage capacity.[7] Apart from it, facile processing, fast switching, good endurance, compatibility with conventional semiconductor processing, and high stability[8–11] make RRAM a promising next generation nonvolatile memory (NVM). RRAM has two stable states, a high resistance state (HRS) and a low resistance state (LRS). The resistive mechanism, such as the conductive filament growth and rupture, has been proved both theoretically[12–14] and experimentally.[15] There are many kinds of materials used as the resistive switching (active) layer, such as transition metal oxides (ZnO,[16] $ZrO_2$,[17] $TiO_2$,[18] NiO,[19] $HfO_x$,[20] $AlO_x$[21]), organic materials,[22] chalcogenides,[23] and so on. However, ordinary RRAM has some problems such as the limitation of electrode thickness, which affects RRAM further scaling down, reading current decreasing in LRS, and flexible fabrication. Recently, 2D material graphene[24] with carbon atoms packed into a plane honeycomb crystal structure becomes a research hotspot due to its extremely high mobility,[25] ease of being scaled down,[26] high light transmittance,[27] strong intrinsic breaking strength,[28] and good electrical and mechanical properties. Many graphene-based devices[29,30] are fabricated, such as transistors,[31] solar cells,[32] sound emitting devices,[33] gas detectors,[34] and photodetectors.[35] Many RRAM problems such as scalability and power consumption can be solved by inserting a graphene layer. Moreover, graphene RRAM owns new exciting properties, for example, high transparency and SET voltage modulation, which will be interpreted in the following. Graphene can be large-area grown both on Cu foil[36] and Ni substrate,[37] which is good news for the mass fabrication of graphene RRAM in the future. Other graphene-based materials are also widely used in RRAM fabrication, such as graphene oxide (GO) and reduced graphene oxide (rGO). GO is a layered stack of the planar, graphene-like sheet decorated by epoxy, diol, hydroxyl, ether, and carboxy groups;[38] and rGO is the reduction of GO by laser scribed,[39,40] chemicals,[41,42] or other methods. Due to easy fabrication, flexible and good electrical, thermal, mechani-

*Project supported by the National Natural Science Foundation of China (Grant Nos. 61574083 and 61434001), the National Basic Research Program of China (Grant No. 2015CB352101), the National Key Research and Development Program of China (Grant No. 2016YFA0200404), the National Key Project of Science and Technology of China (Grant No. 2011ZX02403-002), Special Fund for Agroscientic Research in the Public Interest of China (Grant No. 201303107), the Independent Research Program of Tsinghua University, China (Grant No. 2014Z01006), and Advanced Sensor and Integrated System Lab of Tsinghua University Graduate School at Shenzhen, China (Grant No. ZDSYS20140509172959969).

†Corresponding author. E-mail: yiyang@tsinghua.edu.cn

‡Corresponding author. E-mail: RenTL@tsinghua.edu.cn

© 2017 Chinese Physical Society and IOP Publishing Ltd 

cal, and optical properties, GO and rGO are applied to fabricate all kinds of devices, such as pressure sensors,[43] thermal rectifiers,[44] flexible earphones,[45,46] strain sensors,[47] and light emitters.[48] For RRAM applications, rGO can be used as the electrode and rGO or GO as the active layer, which can achieve RRAM simple fabrication, flexibility, relative good endurance, and high stability. Combining with other materials such as $\pi$-conjugated polymer will improve the RRAM performance and obtain novel properties such as multilevel switching.

In this paper, we will briefly review the different types of graphene-based RRAMs and explore the roles of graphene materials in RRAM application. In Section 2, we give a simple introduction of graphene RRAMs according to the merits and functions of graphene as the electrode, including low power consumption, higher density, monitoring and detecting oxygen ion drift function, transparency, good uniformity, SET voltage modulation, and graphene as the middle layer. In Section 3, GO/rGO RRAM, including rGO as the electrode and GO/rGO as the dielectric layer is reviewed, where the model, metal-insulator-metal (MIM) structure, and GO modification of GO RRAM are included. Finally, we give concluding remarks in Section 4.

## 2. Graphene RRAM

### 2.1. Graphene as electrode

#### 2.1.1. Low power consumption

With the integration scale becoming larger, low power consumption for single RRAM is essential. Large out-of-plane resistance caused by the weak interaction of graphene with other materials[49] can meet the need. References [50] and [51] used single layer grapheme (SLG) to engineer the interface between the oxide layer and the metal electrode and reduce the RESET current, providing a potential way towards further lowering the programming energy of RRAM.

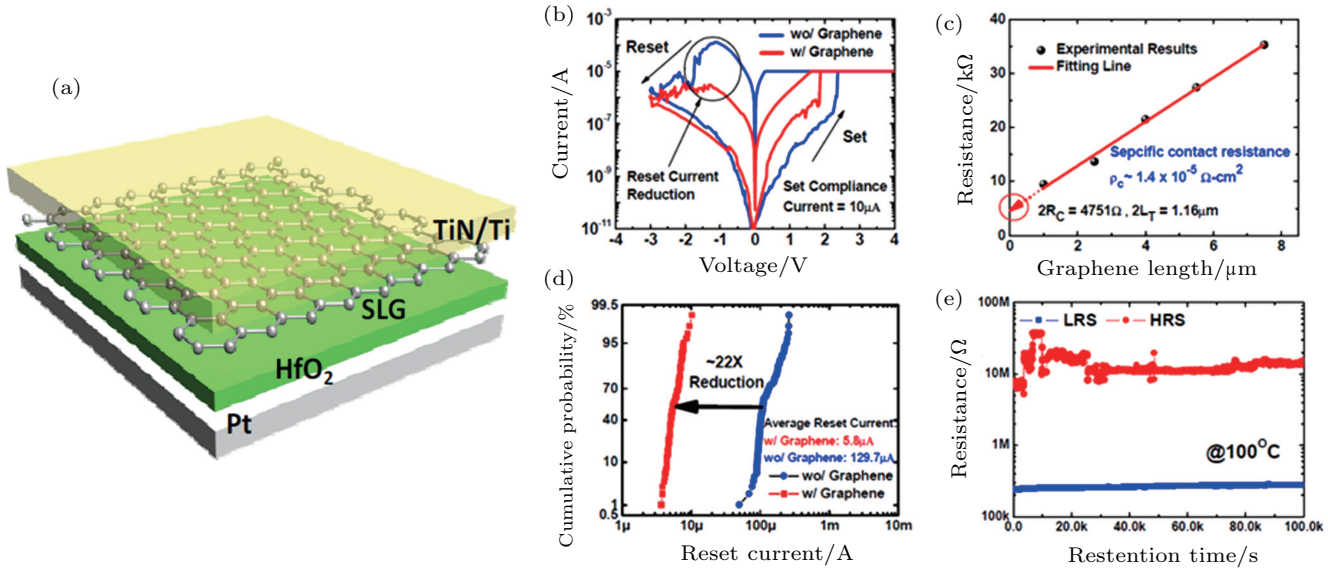



**Fig. 1.** (color online) (a) The structure of Pt/HfO$_x$/graphene/Ti/TiN RRAM. (b) The *I*–*V* curves of RRAMs with and without graphene, showing that the GRRAM owns lower SET voltage and RESET current. (c) The relation between the contact resistance between graphene and the top electrode and the graphene length, indicating low contact resistance with the top electrode. (d) The relation between the cumulative probability and the RESET current of RRAMs with and without graphene respectively. The RESET current of RRAM with graphene has a 22 reduction compared to that without graphene. (e) Retention time of GRRAM under HRS and LRS, repectively. The figure is reproduced from Ref. [51].

The structure is shown in Fig. 1(a), composed by Pt/HfO$_2$/SLG/Ti/TiN. The thickness of the insulating layer (HfO$_2$) is $\sim$ 5 nm and TiN/Ti is $\sim$ 65 nm/8 nm. The specific contact resistivity (Fig. 1(c)) between SLG and the top electrode is $\sim 1.4\times10^{-5}$ $\Omega\cdot$cm$^{-2}$, showing a good contact between them. Compared with the sample without SLG, this RRAM reveals a high-resistance interface barrier ($>$ 900 k$\Omega$) and shows 22 times smaller average RESET current as shown in Fig. 1(d). The programming power consumption (calculated as the RESET voltage multiplied by the peak of the RESET current) shows $\sim$ 47 times reduction for SLG RRAM. Over $10^5$ s retention time can be realized (Fig. 1(e)).

#### 2.1.2. Monitoring and detecting oxygen ion drift

Theoretical researches suggest that the switching mechanism for oxide-based RRAM is oxygen ion drift caused by external electrical field. However the redox reaction caused by oxygen ion drift occurs beneath the top electrode, which is hard to analyze and monitor with a nondestructive method for ordinary RRAM. The graphene RRAM coupled with Raman spectroscopy or XPS will be an effective way to solve the problem since the different state of oxygen ion drift in RRAM will cause the change of graphene Raman and XPS spectra.

For graphene Raman spectroscopy, the G peak shift and 2D peak intensity change can reflect the doping effect in

the graphene.[52] Therefore observing these two parameters changing during the graphene RRAM SET/RESET process can monitor and detect oxygen ion drift.[51] As shown in Fig. 2, the G peak position after RESET is left shifted compared to that after SET, indicating the p-type doping becomes lighter. The intensity of the 2D peak is a function of the switching cycle and in each cycle, the 2D peak intensity of SET is always lower than that of RESET. These changes are mainly from the doping changes caused by the migration of oxygen ions. During the SET process, oxygen ions move and diffuse laterally toward graphene under the applied electrical field until they form covalent bonds with DB defects existing on the SLG surface. This process makes graphene p-type doping, which will increase the wave number of the G peak and decrease the intensity of the 2D peak and the resistance of SLG will be reduced.[53] During the RESET process, under the reversed external electrical field, oxygen ions move back to the oxide layer. This process would change the graphene towards intrinsic doping, leading to a decrease of the wave number of the G peak and an increase of the intensity of the 2D peak.

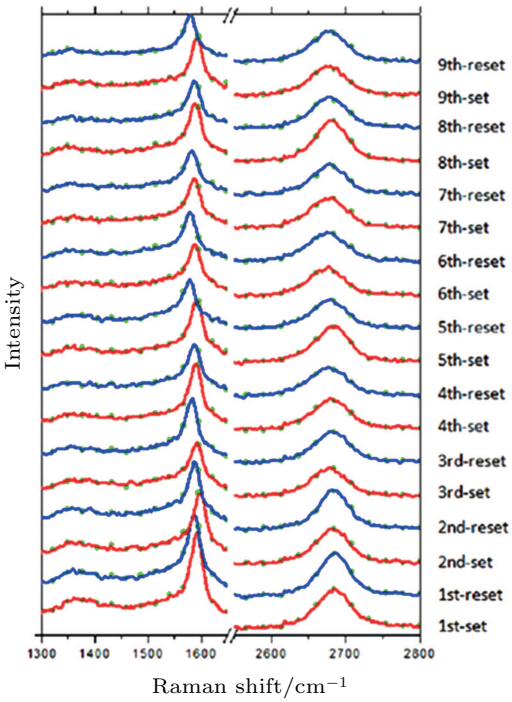



**Fig. 2.** (color online) The change of graphene G peak and 2D peak Raman shift after repeating the SET and RESET process. The figure is reproduced from Ref. [51].

XPS is a more convincing method to detect the oxygen ion drift as it can directly observe the covalent bond type change during the graphene RRAM SET/RESET process. Reference [54] fabricated SLG/Pt/$Al_2O_3$($\sim$ 1 nm)/$TiO_2$/Pt RRAM and tested its XPS spectra of C 1s, O 1s, Ti 2p, and Al 2s binding states at HRS and LRS, respectively. The LRS is achieved by the SET process under a negative bias, which causes the formation of a $TiO_x$ suboxide at the $TiO_2$ surface. After the RESET process, the bond fraction of C–O/C=O increases while that of the $Ti^{3+}$ BE state decreases. $O^-$ ions drift toward the SLG/$Al_2O_3$ interface and are assumed to convert to the surface Al–OH to Al–O bonds partially. Therefore, $Al^{3+}$ in Al–O is decreased in LRS compared to that in HRS. From the above XPS analysis, we can figure out that the oxygen ions from the bottom side of the $TiO_2$ layer are activated to move to the upper side by a positive bias applied, cross over the ultrathin $Al_2O_3$ layer, and bond with the SLG finally.

### 2.1.3. Higher density

In order to achieve high density RRAM, 3D RRAM using the edge of the 3D stacked metal plane as one of the RRAM electrodes is becoming prevalent in this field. But in order to make higher density RRAM, the total stack height (metal and dielectric) must be scaled down due to limitations of the etch aspect ratio.[55] Owing to graphene ultrathin thickness and excellent electrical conductivity, 3D RRAM using graphene as the electrode plane as shown in Fig. 3 will dramatically lower the height for single RRAM and make the density much higher than that using ordinary metal (such as Pt) without sacrificing RRAM performance.[56] It is assumed that if the top electrode trench has an 89° slope, the 3D RRAM can achieve up to 200 stacks. This memory window of G-RRAM is significantly ($> 10\times$) larger than that of Pt-RRAM, which is attributed to ultrathin CF formed from the edge of the ultrathin graphene electrode. If the same methodology for the worst-case selected cell of 3D RRAM as in Ref. [57] is used to test with the criteria of a 75% write access voltage margin and an over 100 nA read margin, an array size of $>$ 100 G for a 200-stacked graphene RRAM can meet both criteria, while an array less than 100k Pt-RRAM can only reach the read margin criterion. It is because lower height for 3D graphene RRAM results in overall low pillar resistance in a 3D stack architecture with cross point structure, which makes higher density 3D GRRAM more competitive in practical applications.

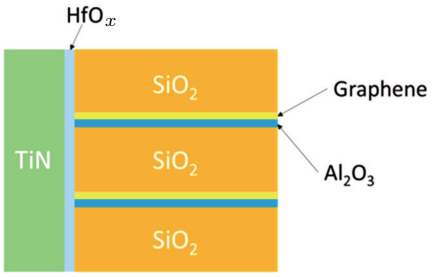



**Fig. 3.** (color online) The structure of graphene 3D stacked RRAM.

### 2.1.4. Well performed transparent electrode

Only $\sim$ 2% light is absorbed by graphene,[58] therefore graphene has the huge potential of being a transparent circuit used in electrode application. Compared to ITO-based transparent RRAM (TRRAM), using graphene as the RRAM transparent electrode not only gets high light transmittance in the

large wavelength, but also improves the RRAM performance. For example, the graphene sheet resistance ($\sim 30\ \Omega/\square$) is much lower than ITO[59] and the graphene/ZnO TRRAM[60] SET voltage ($< 1$ V) is much lower than that without graphene ($\sim 3$ V), and the sudden drop of leakage current in both SET and RESET processes will not happen, showing graphene-based TRRAM reversible and steady bipolar switching characteristics. Moreover, graphene can eliminate an undesired surface effect better and as a result a high yield of graphene RRAM can be obtained. The ordinary ITO/ZnO/ITO device exhibits a relatively low switching yield in a vacuum and $O_2$ ambience (41.7% and 50.0%, respectively) as compared to the device in the ambience of $N_2$ and air (66.7% and 58.3%, respectively). However for graphene-based devices, the switching yield is greatly increased in all four cases (66.7%, 66.7%, 75.0%, and 75.0% in a vacuum, $O_2$, air, and $N_2$, respectively) and insensitive to the environmental atmosphere, indicating that the graphene can be not only a transparent electrode material but also a passivation layer due to the weak chemisorption of $O_2$ molecules.[61]

For graphene ZnO TRRAM, a forming process is needed, but if the dielectric layer is changed into a rare-earth-oxide-based thin film, the forming process is not necessary owing to its forming-free characteristics.[62–64] Reference [65] fabricated multilayer grapheme(MLG)/$Dy_2O_3$/ITO TRRAM with 80% transmittance at 550 nm. $Dy_2O_3$ has a direct and wide bandgap of $\sim 5.5$ eV at room temperature, which meets the intrinsic transparency requirement in resistive switching materials without sacrificing the memory density or capacity.[66] Due to excellent properties of the transparent electrode, the device exhibits unipolar resistance switching with low operation voltage ($< 1$ V), low operation current ($< 100$ μA), low power consumption ($< 100$ μW), high resistance ratio ($> 10^4$), reliable data retention, fast switching speed ($< 60$ ns), and promising cycle endurance ($> 200$ cycles), exhibiting the strong competitiveness with graphene TRRAM for which the forming process is needed.

### 2.1.5. Good uniformity

Uniformity measures the uniform level of parameters such as the resistance distribution in HRS or LRS. Long operational RRAM lifetime is dependent on it. Inserting graphene between the metal and dielectric will improve the RRAM uniformity, for example, Al/graphene/$VO_x$/Cu RRAM[67] exhibits a good resistive switching at low current compliance ($\sim 2$ mA) while $VO_x$ RRAM without graphene needs a large one ($\sim 20$ mA). Although a little larger resistance distribution in LRS exists for the graphene-based RRAM compared to that without graphene, the uniformity of HRS is greatly improved, which indicates that the overall uniformity of $VO_x$ RRAM has been improved by using the embedded graphene.

### 2.1.6. Lowering SET voltage

With the integrated circuit scaling down, the supply voltage must be reduced correspondingly. Low SET voltage for RRAM is requested if it is integrated with other circuits. For some dielectrics such as NiO, the graphene will form a Schottky contact with it and enhance the electrical field intensity in the resistive switching layer, which will help the CF grow. As a result, the dielectric/graphene-based RRAM will own the lower SET and RESET voltages compared with that without graphene.[68]

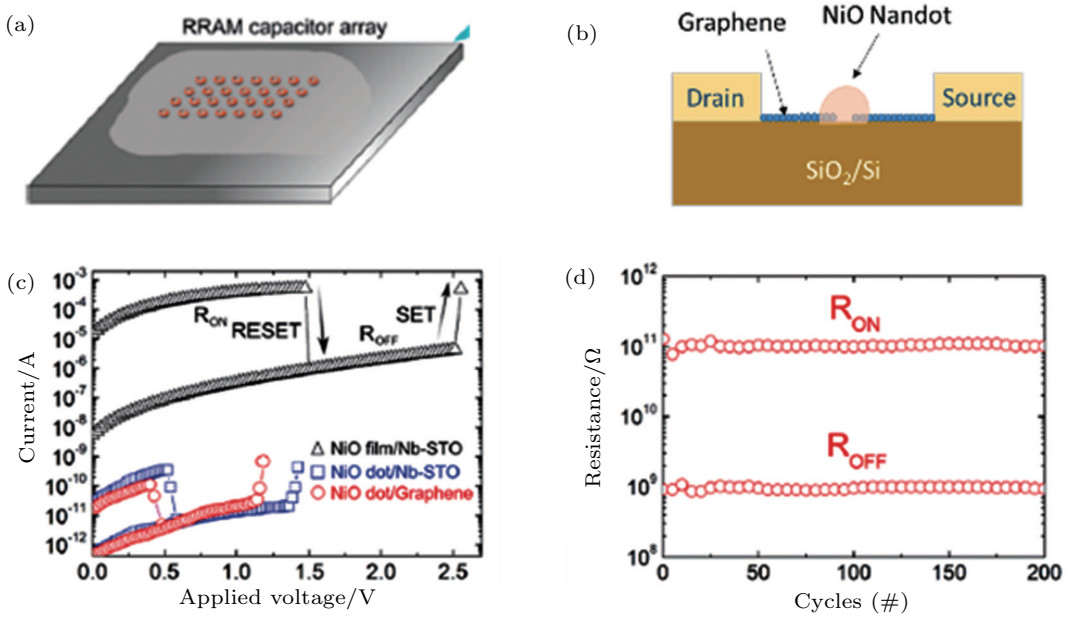



**Fig. 4.** (color online) NiO/graphene RRAMs with (a) vertical and (b) plane structure. (c) *I*–*V* curve comparison among RRAMs fabricated with NiO film, NiO dot, and NiO dot/graphene in vertical structure. (d) The repeating test results in vertical structure. Panels (a), (c), and (d) are reproduced from Ref. [69].

Reference [69] used an anodic aluminum oxide (AAO) nanotemplate for the formation of the NiO RRAM nanocapacitor (Pt/NiO/graphene capacitor) array as shown in Fig. 4(a). The pore diameter in the nanotemplate is about 30 nm and the interpore distance is about 100 nm. The device is a vertical structure and exhibits the typical unipolar RRAM switching behavior with ON current below 1 nA, and as Fig. 4(c) shows, it has lower SET ($\sim 1.2$ V) and RESET ($\sim 0.4$ V) voltages than those on the surface of Nb-doped $SrTiO_3$ no matter for the NiO RRAM nanocapacitors (1.5 V for SET and 0.5 V for RESET ) and the NiO thin film RRAM (2.5 V for SET and 1.5 V for RESET). Despite the work function of graphene (4.66 eV) being higher than that of Nb-doped SrTiO3 (4.2 eV),[70] the NiO/graphene Schottky contact is supposed to contribute to the lower SET and RESET voltages of the graphene NiO RRAM.

Reference [71] provided a plane structure with graphene nanoribbon (GNR)[72] as the electrode and the NiO nanodot covering the $\sim 25$ nm width GNR nanogap as the switching layer, as shown in Fig. 4(b). The fabrication of monolayer graphene nanoribbon and deposition of the NiO nanodots onto the GNR nanogap are achieved by polystyrene dip-pen nanolithography (DPN). For this device, the SET and RESET voltages are $\sim 1.2$ V and 0.4 V, respectively, which are similar to those with the vertical structure. Both vertical and plane structures own good reproducible switching behavior. After 200 switching cycles, the resistances of HRS and LRS change little for both devices.

### 2.1.7. Modulating SET voltage

A-B stacked bilayer grapheme (BLG) can open the bandgap by an external electrical field,[73–76] which is different from single layer graphene with zero bandgap. For RRAM, this bandgap can be used to control the intensity of the electric field in the resistive switching layer and in turn, adjust the SET voltage.

Due to that the bandgap is determined by the external electrical field, extra bottom dielectric and gate electrode are needed. The structure in Ref. [77] is shown in Fig. 5(a). The main body of RRAM is Al/$AlO_x$/BLG/Au and the voltage applied on the high doping Si substrate is used to provide an electrical field to open the BLG bandgap. When the gate voltage changes from $-35$ V to 35 V, the SET voltage for RRAM will increase from 0 V to 4.1 V (Figs. 5(b)–5(d)), indicating that the SET voltage has a positive correlation with the gate voltage. It is because that for positive gate voltage, the bandgap will open and allow the electrical field from the gate to cross over the BLG into the resistance change material. The device enters the oxygen ions depleted state and the CF forming is prevented by the electrical field. In order for oxygen ions to screen the electrical field from the gate, the SET voltage is required to be higher to excite more oxygen ions and then form the CF. On the other side, the device enters the oxygen ions accumulated state for negative gate voltage. The bandgap is also opened and renders the electrical field to pass though BLG into the resistance switching layer, which in turn attracts more oxygen vacancies. As a result, the CFs could be formed under a lower SET voltage. By this mechanism, the gate voltage achieves the modulation of the SET voltage.

The HRS/LRS ratio is also changed with the gate voltage, from $10^3$ at $-35$ V to $10^5$ at 35 V. It can be interpreted as that under a negative gate voltage, the oxygen vacancies will be attracted, resulting in the resistance decreasing of HRS and the HRS/LRS ratio. Conversely, under a positive gate voltage, some oxygen ions will be depleted, leading to the resistance increasing of the HRS and the HRS/LRS ratio.

Compared with the conventional one-diode-one-RRAM (1D1R) structure where the diode is used as a selector, this BLG RRAM can use the gate as the selector and owns the low OFF current, easy to achieve high density 3D stacking, and more compact merits.

### 2.1.8. Multilevel resistive switching

Multilevel switching has a great potential for RRAM on industrial memory applications.[78–81] Using graphene as an electrode can also achieve stable and repeatable multilevel resistive switching behavior. Reference [82] used nanographene (NG) and nanogap to achieve RRAM multilevel switching. NG owns many appealing properties, such as tunable conductivity, scaled-up capability of integration, facile device fabrication, and fabrication compatible with modern CMOS technology, which make it very suitable to use as an electrode.

The device structure is similar to a back-gate nanographene transistor in its original state. By applying a certain voltage, a forming process between the two electrodes activates its resistive switching behavior in the new device. After the forming process, the electrical breakdown occurs and the nanogap appears in the middle of nanographene due to Joule heating.[83] This nanogap is served as the switching layer of RRAM.

The device shows unipolar resistive switching behavior. The SET voltage is $\sim 2.8$ V and the RESET voltage is $\sim 5.5$ V, an over $10^3$ ON/OFF current ratio can be obtained at 1 V. The reversible reduction and oxidation of these silicon nanocrystallites in the $SiO_2$ layer and the FN tunneling current[84] controlled by the external applied voltage are the key to the resistance switching effect during the SET and RESET procedures.

By changing the RESET voltage sweeping scope, the device shows multilevel switching properties. The resistance in HRS is relevant to the maximum sweeping voltage. When applying 3 V, 5 V, 7 V, 9 V, and 11 V bias pulses, the resistance changes to different values and varies widely. Besides the retention time can be up to $10^4$ s, showing a very good stability.

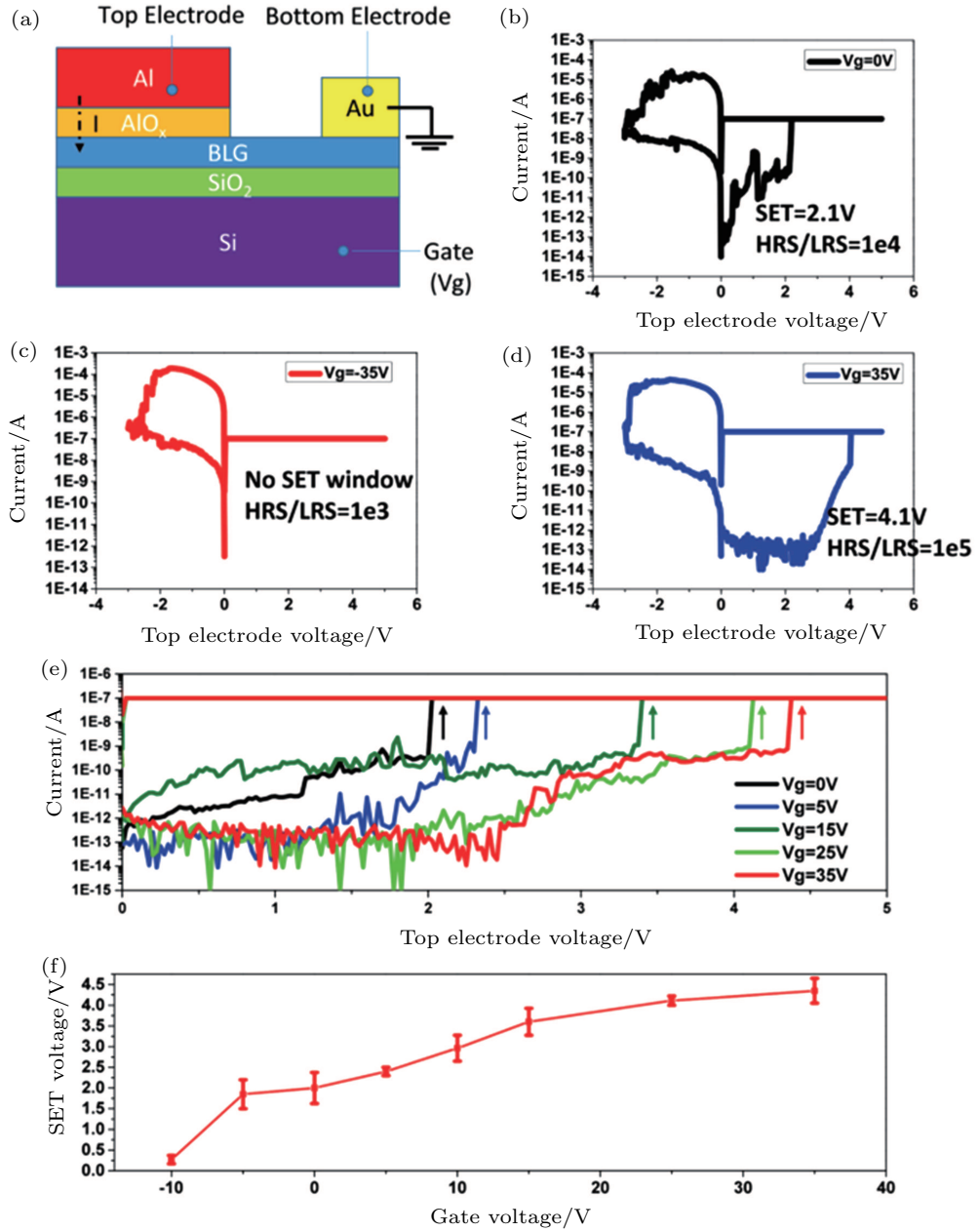



**Fig. 5.** (color online) (a) The structure of gated Al/$AlO_x$/BLG/Au RRAM, where Al is used as top electrode, Au as bottom electrode, and Si as gate electrode. (b)–(d) *I*–*V* curves at different gate voltages, indicating the SET voltage and HRS/LRS ratio modulated by the gate voltage. (e), (f) The SET voltage changing trend varying with the gate. The figure is reproduced from Ref. [77].

### 2.2. Graphene as middle layer

For some RRAM devices, graphene is sandwiched between two dielectrics and served as the trapping site and is able to generate a local internal field to help filament grow, especially for an organic layer which is usually very thick and makes the external electrical field too weak to form a filament in it. For instance, the structure ITO/PMMA/GFs/PMMA/Al[85] shows great electrical bistable resistive switching property even the test temperature is up to 150 °C, $10^3$ ON/OFF state current ratio and $10^5$ s switching cycles can be obtained without obvious ON and OFF state degradation, which exhibits relatively large switching windows and good stability.

Apart from that, graphene as the middle layer is usually utilized for achieving multilevel switching, which is similar to Subsection 2.8, however the graphene is no longer used as an electrode but as a trapping site. Reference [86] fabricated organic RRAM with graphene nano flakes (GF) which are a good charge trapping[87] and storage[88] medium. This device uses polyvinylidene fluoride (PVDF) as the switching layer because of its better heat resistance, non-reactive nature, low weight, and flexibility. ITO on glass substrate is used as the bottom electrode. Two PVDF polymer layers are fabricated through the spin coating process and GR is obtained from GO by using reducing agent hydrazine monohydrate. The *I*–*V* curve shows double set and reset property. As the voltage increases, the current is growing but still in the OFF state. The index for the *I*–*V* curve is $\sim 2$, which indicates that the space

charge limited conduction (SCLC) mechanism[89] dominates the process. When the voltage reaches $\sim 1.8$ V, the current suddenly rises and the resistance state jumps to an intermediate low resistance state from HRS. With voltage further going up, the second current jump occurs at $\sim 2.2$ V and the device enters the total low resistance state. On the contrary, if a negative voltage applies on the device, the small current jump-down happens at $-2.3$ V and the large one happens at $-2.9$ V as the negative voltage becomes larger. The device finally enters the high resistance state.

The explanation of this phenomenon can be interpreted as follows. When a positive voltage is applied on the top gate, the electrons from the ITO electrode will be injected into the lowest unoccupied molecular orbital (LUMO) level of PVDF. As the voltage increases, these electrons sourced from the ITO electrode are captured by the electron trap nodes existing in GR. Once the graphene trapping sites are almost occupied by electrons, they can generate an electrical field strong enough to form a conducting path in the film and make the device transfer from HRS to LRS. The double SET process may attribute to the formation of multichannels with different trapping threshold potentials. On the contrary, when the applied voltage is reversed, it will de-trap the electrons from the graphene trapping sites and eject them back to the ITO electrode. Decreasing the voltage down to some degree, the conducting channel will be disconnected and the current will suddenly jump down. After all channels are broken down, the device will enter the total OFF state. Owing to it, the formation of extra conducting channels can be manipulated by limiting the current flow. Therefore controlling the compliance current can be used to achieve multi-bit storage. For this device, different LRS can be observed with different compliance current and at a certain reading voltage, multi-LRS is able to read out. In addition, multilevel switching can also realized by applying different SET and RESET pulses.

## 3. GO/rGO RRAM

### 3.1. rGO as electrode

rGO is a special kind of graphene which is reduced from GO, the thin rGO film behaves as graphene, therefore rGO can be used as the electrode as graphene is. Reference [90]

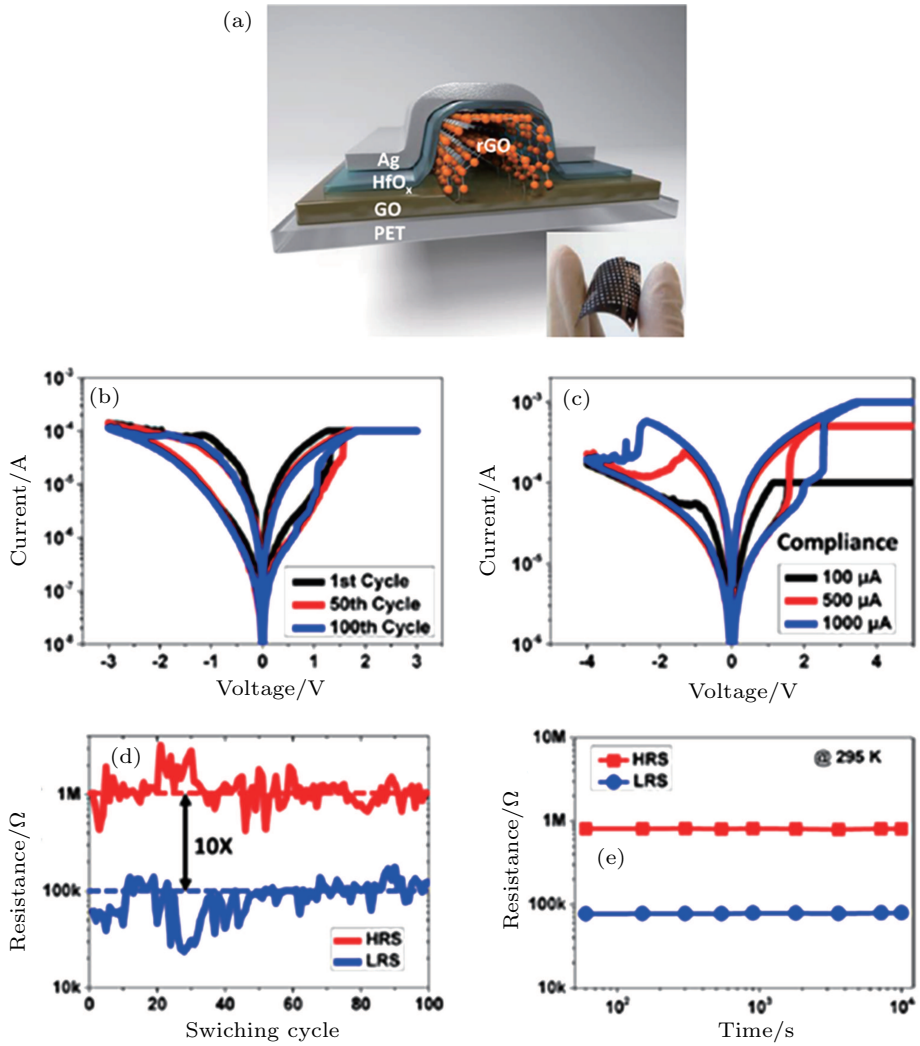



**Fig. 6.** (color online) (a) The structure of Ag/$HfO_2$/rGO RRAM on PET substrate. (b) *I*–*V* curve of the device in the first cycle, 50th cycle, and 100th cycle. (c) *I*–*V* curve of the device under different current compliance, showing the potential for multilevel switching application. (d) The switching cycle test of the device in HRS and LRS. (e) The endurance test of the device. The figure is reproduced from Ref. [90].

used the laser-scribed technology to reduce GO to rGO (or laser-scribed grapheme (LSG)) and fabricated RRAM with rGO as the electrode, as shown in Fig. 6(a). The device is fabricated on a polythylene terephthalate (PET) flexible substrate, thus it has potential to be integrated into a flexible circuit. The forming voltage ($\sim$ 1 V) is comparable to the devices' SET voltage ($\sim$ 1.2 V for the first SET), indicating that the device is forming free.[91] The ON/OFF current ratio is $\sim$ 10 due to the large HRS resistance. Under different current compliance, the device shows the potential of multi-level switching application. The retention time is over $10^4$ and little degradation can be observed after 100 cycles, showing good reliability.

By changing the material of the top gate from Ag to Pt (Figs. 7(c) and 7(d)) and conducting Ag-based RRAM LRS resistance temperature test as Fig. 7(a) shows, the Ag ions movement is confirmed as playing a dominant role in the growth of the conductive filament. The phenomenon of LRS resistance changing with temperature variation means that the filament growth is unlikely to be relevant to the oxygen vacancy.[92] High LRS resistance between 42 °C and 50 °C is attributed to the composite outcome between the electron scattering increasing and diameter of metal filament reduction as the temperature goes up. The high SET voltage of Pt-based RRAM further confirms that the Ag ions form filaments in Ag-based RRAM since that Pt cannot diffuse into $HfO_2$ and it needs a high voltage for the oxygen vacancy to form the filament.

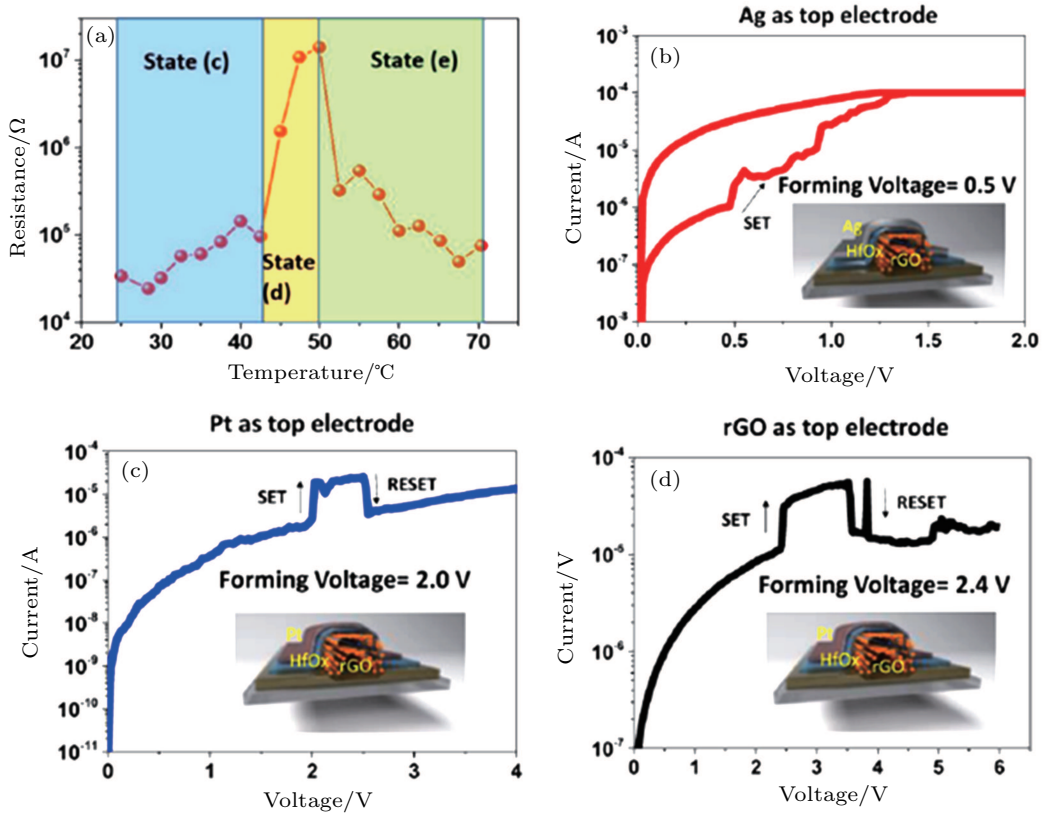



**Fig. 7.** (color online) (a) The relation between the resistance in LRS and temperature in Ag/$HfO_2$/rGO RRAM. (b) The forming process for the Ag-based RRAM, indicating low forming voltage needed. (c), (d) *I*–*V* curves of Pt/$HfO_2$/rGO under Pt and rGO as top electrode, respectively. The figure is reproduced from Ref. [90].

### 3.2. GO/rGO as dielectric

As Section 1 describes, GO film is cost-effective, easy to fabricate, flexible, etc. which is suitable to make low lost, flexible graphene circuits. For RRAM, GO is usually used as the switching layer and the simplest structure is the typical MIM structure: metal/GO/metal,[93] or MIS structure: metal/GO/semiconductor.[94] In GO MIM structure, a large range of metallic materials can be used as the electrode, such as metal elements, indium-tin-oxide (ITO),[95,96] and even grapheme.[97]

#### 3.2.1. Model

When GO/rGO is used as dielectric, it becomes the place where the resistive switching happens. However, the mechanism of resistive switching in GO and rGO is different from that of conductive filament growth in most ordinary RRAMs. Therefore the accurate modeling of RRAM with GO/rGO as dielectric is very essential to have a deep understanding of its resistive switching behavior. For most of GO RRAMs published and introduced in the following section, the following reviewed models (such as space–charge-limited current model and Ohmic current model) are used widely to simulate GO/rGO RRAM.

Several models of GO and rGO have been proposed and ascertained.[98–100] For RRAM, the potential difference between two electrodes will drive the $sp^3$ and $sp^2$ mutual conversion, which will increase or decrease the concentration of $sp^2$ clusters and thus decide the conductivity of the GO film. The $sp^2$ clusters growth rates can be express based on phenomenological Butler–Volmer kinetics[101] as

$$\begin{cases} \upsilon_{\rm red} = k_0 \exp\left(-\dfrac{\Delta rG_0 + \alpha ZF\eta}{RT}\right), \\ \upsilon_{\rm OX} = k_0 \exp\left(-\dfrac{\Delta rG_0 - (1-\alpha)ZF\eta}{RT}\right), \\ \upsilon_{\rm C} = \upsilon_{\rm red} - \upsilon_{\rm OX}, \end{cases} \tag{1}$$

and the mechanism of electron transport between GO layers can be described by the multiphonon trap-assisted tunneling (MTAT) model[102] as

$$\begin{cases} R_{\rm c} = \tau_{\rm c}^{-1}(x) N_{\rm t}(1-f_{\rm t}), \\ R_{\rm e} = \tau_{\rm e}^{-1}(x) N_{\rm t} f_{\rm t}, \end{cases} \tag{2}$$

where $\upsilon_{\rm red}$ , $\upsilon_{\rm OX}$, and $\upsilon_{\rm C}$ represent the net reaction rates of the GO reduction process ($sp^3$ to $sp^2$ conversion), GO oxidation process ($sp^2$ to $sp^3$ conversion), and total $sp^3$ to $sp^2$ conversion, respectively; $k_0$ is the kinetic constant of the electrochemical reaction, $\alpha(=0.5)$ is the asymmetry factor, $\Delta rG_0$ is the free energy of the reaction at equilibrium, and $F$ is the Faraday constant. $Z$ is the charge-transfer number and $\eta$ is the redox overpotential and can be estimated as the negative absolute of the applied voltage.[103] $R$ and $T$ are the ideal gas constant and temperature, respectively. For the MTAT model, $N_{\rm t}$ and $f_{\rm t}$ are the spatial density and the electron occupation probability of the trap, respectively. $\tau_{\rm c}^{-1}(x)$ and $\tau_{\rm e}^{-1}(x)$ are the time constants for the electron capture and emission. $R_{\rm c}$ and $R_{\rm e}$ are the capture and emission rates.

Equation (1) can be simplified as an Arrhenius-like[104] equation

$$\upsilon_{\rm C} = \upsilon_0 \exp\left(-\frac{E_{\rm act}}{kT}\right) \sinh\left(\frac{ZqV_{\rm cell}}{2kT}\right), \tag{3}$$

which is similar to the filament growth rate in ordinary RRAM, where $E_{\rm act}$ is the amorphous carbon activation energy ($\sim 3.5$ eV), $\upsilon_0$ is the fitting parameter, and $V_{\rm cell}$ is the applied voltage.

The following space–charge-limited current (SCLC) model[105] is used to describe the current characteristics in HRS:

$$J = \frac{A\mu\varepsilon}{d^3} V^2 \exp\left[\left(\frac{0.891}{kT}\sqrt{\frac{q^3}{d\pi\varepsilon}}\right) V^{1/2}\right], \tag{4}$$

which can be simplified as $J \approx \alpha V + \beta V^2$, where $J$ and $V$ are the current density and the applied voltage, respectively, $A$ is a positive constant, $\mu$ is the charge carrier mobility, $\varepsilon$ and $d$ are the permittivity and the thickness of the GO film, and $k$ and $q$ are the Boltzmann constant and the unit electron charge, respectively. The Ohmic current model is used to fit the current in LRS due to the fact that the conductivity of the device in LRS is very large, the device in LRS can be simply treated as a simple linear resistance. These two models can fit the experimental data very well[106] and prevail in the GO RRAM theoretical analysis.

### 3.2.2. MIM structure GO RRAM

The first reported GO RRAM is the structure Cu/GO/Pt,[107] the thickness of GO by the vacuum filtration method is $\sim 30$ nm. Apart from easy fabrication, the major merit of the device is the low switching voltage. The SET voltage distributes in the range from 0.3 V to 1 V and the RESET one is from $-0.3$ V to $-0.9$ V. Low SET and RESET voltages contribute to the diffusion of the top electrode under an external voltage and the adsorption/release of oxygen-related groups during the formation and rupture of conductive filament in the GO film. The current ON/OFF ratio is only 20, which is not very good, indicating that the GO resistance in HRS is not high enough. The retention time is more than $10^4$ s and after 100 switching cycles, no obvious degradation of the ON/OFF ratio is observed, showing a relatively good stability.

Due to the flexibility of the GO film, RRAM can also be fabricated flexibly. Reference [108] proposed Al/GO/Al flexible RRAM as shown in Fig. 8(a), which is on the flexible polyethersulfone (PES) substrate. The GO film is fabricated by a simple and scalable spin-casting process[109] with GO solution and by this method, the GO film can be made large-area uniform and transferred in any kind of substrates. The device shows bipolar switching behavior and the ON/OFF ratio can reach up to 100 (Fig. 8(b)), smaller than that of the ordinary RRAM. But the retention time is over $10^5$ s, competitive with the conventional one. After 100 switching cycles, the HRS/LRS memory window shows no noticeable degradation, which exhibits good stability and repetitiveness. The yield for this GO RRAM device is near 80%, which is good news for mass manufacture. It is noticed that the device shows negative voltage SET and positive voltage RESET and forming free characters. The resistive switching voltage is $\sim 2.5$ V, a little higher for graphene-based RRAM.

The device shows good flexibility. When the bending radius enters the extremely flexed state ($\sim 7$ mm for the device), the current ON/OFF ratio can also be maintained as the degree of flat device as shown in Fig. 8(d). The resistive switching also results from filament growth. By the assistance of atomic-resolution TEM and energy-filtered TEM (EFTEM),[110] the filament is directly observed to be formed and de-formed in the very thin insulating layer at the top Al/GO interface under different applied voltages, rather than in the bulk film.

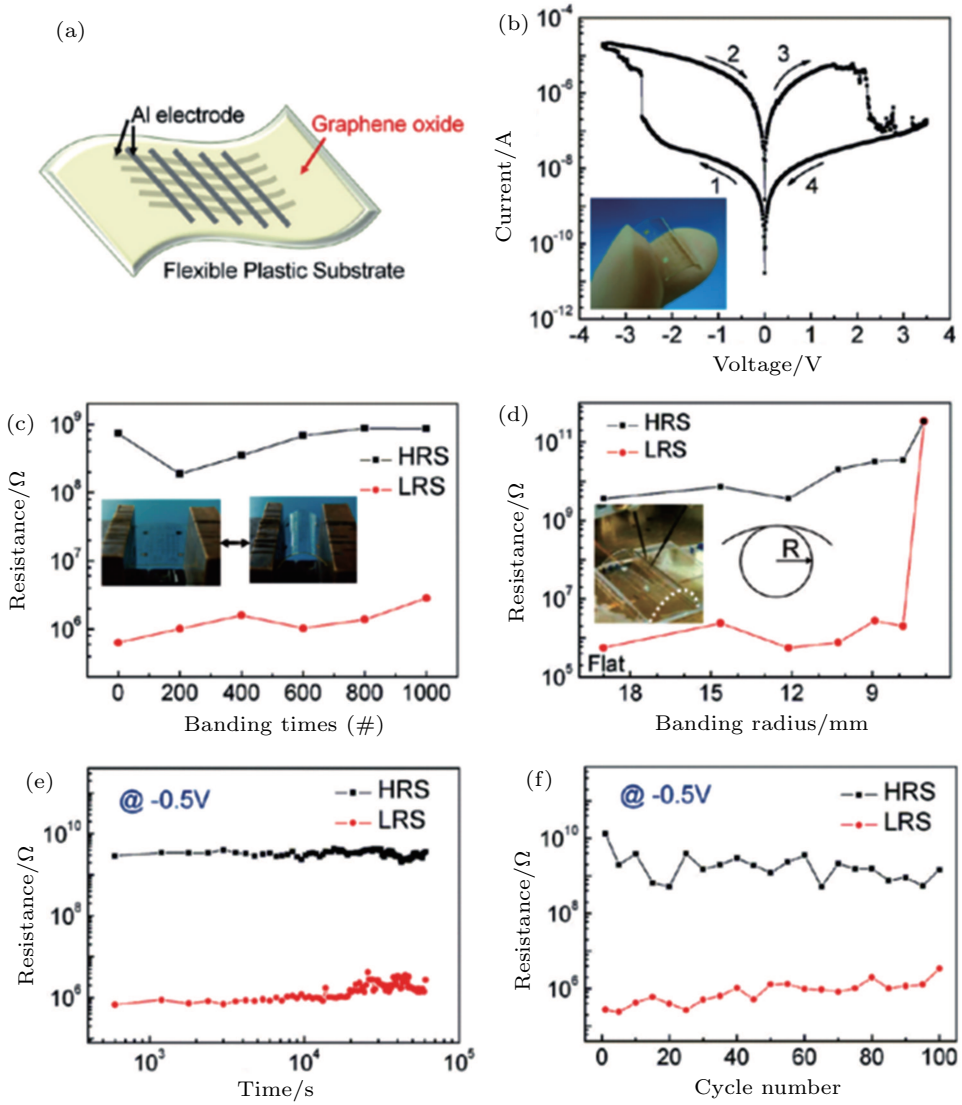



**Fig. 8.** (color online) (a) The structure of flexible Al/GO/Al RRAM. (b) *I–V* curve of the device. (c) The bending time test for the RRAM. (d) Bending radius test in HRS and LRS. (e) The retention properties of the RRAM. (f) The endurance properties of GO RRAM. The figure is reproduced from Ref. [108].

Other GO RRAMs with MIM structure have been deeply researched as well, such as metal/GO/Pt.[111] In a relatively large proportion of these RRAMs, the metal electrode ions diffusion dominates the filament growth and anticlockwise (AW) bipolar switching. They show good retention time (over $10^3$ s) and cycle number ($> 100$), exhibiting high stability and well repeatability.[112] However, the type of electrode has a profound effect on the switching voltage and yield of GO RRAM. Taking metal/GO/Pt RRAM as an example, the metal here can be Ag, Ti, Cu, Au, etc. The forming voltages for these four metal RRAMs vary as follows: $V_{\rm Ag} < V_{\rm Ti} < V_{\rm Cu} < V_{\rm Au}$ . Compared to other metals (Ag, Ti, Cu), gold needs a high voltage to be oxidized to ions and activate Au/GO/Pt RRAM. The yields of these RRAMs vary as follows: $Y_{\rm Ag} > Y_{\rm Cu} > Y_{\rm Au} > Y_{\rm Ti}$.[111] Ag-based GO RRAM has the maximum yield (reach up to $\sim 70\%$) and the lowest forming voltage among the four devices, indicating that Ag can be treated as the selective electrode for GO RRAM application.

### 3.2.3. RRAM with modified GO

For metal/GO/ITO RRAM, many modifications of GO have been made to improve the RRAM properties such as lower the SET voltage. One modification method is adding one more layer above or below the GO film. For example, reference [113] proposed $Pr_{0.7}Ca_{0.3}MnO_3$ (PCMO)/GO RRAM by inserting PCMO between GO and the bottom electrode to realize oxygen exchange between GO and the PCMO layer, as shown in Fig. 9(a). PCMO owns a higher oxygen vacancy concentration at the surface region and can be used as a good ion conductor.[114] Both GO and PCMO films are deposited by a spin coating method at low temperature (300 ° ), annealed at 250 °C for 1 h and 150 °C for 30 min respectively after spin-coating. After that, Pt is deposited as the top electrode. This device shows reverse bipolar switching behavior. Due to PCMO high oxygen vacancy concentration, the oxygen in GO is inclined to move to the surface of PCMO, which is assumed to contain 5% higher oxygen vacancies than the bulk

region,[115] making both GO and PCMO more conductive and therefore less voltage (−0.75 V for SET as Fig. 9(b) shows) is needed to achieve switching. Apart from that, the ON/OFF current ratio of the device is $\sim 10^2$, the normal operating cycles can be up to 150, exhibiting good stability. As Fig. 9(d) shows, the retention time is up to $10^4$ s even at test temperature 85 °C, showing good store retention property at high temperature.

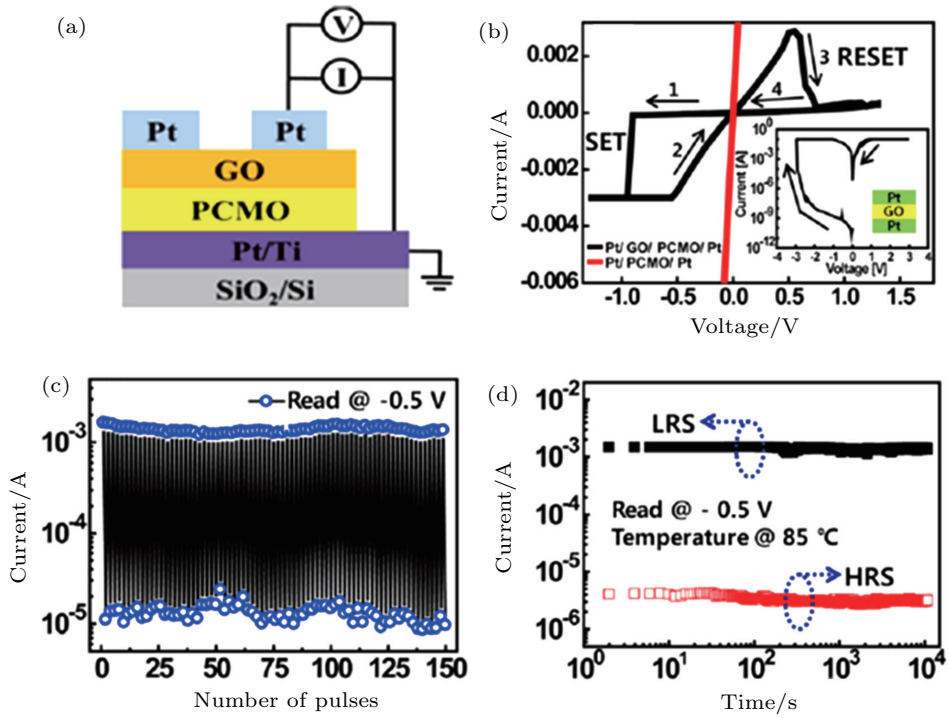



**Fig. 9.** (color online) (a) The structure of PCMO/GO RRAM. (b) *I*–*V* characteristics of this device. The inset is *I*–*V* properties of RRAM without PCMO layer, which has a large SET voltage. (c), (d) Repeatability and endurance properties of PCMO/GO RRAM in HRS and LRS. The figure is reproduced from Ref. [113].

Another modification method is to make a GO composite film with other materials. The added materials can be classified as three types: nanoparticle (NP), polymer, and 2D materials such as $MoS_2$. The following part will introduce the three types of materials in detail.

**(i) Polymer** The factionalized GO and $\pi$-conjugated polymers composites have been explored as the switching layer in RRAM to achieve high ON/OFF current ratio, high stability, and lower switching voltage. For example, reference [106] presented soluble triphenylamine-based polyazomethine (TPAPAM)-GO RRAM which shows low SET voltage and high stability. The RRAM structure is ITO/TPAPAM-GO/Al. Similar to the role of PCMO in PCMO-GO RRAM, the TPAPAM is used as the hole-transport agent due to its low ionization potential, high mobility, and excellent hole injection. This device shows reverse bipolar switching property. The SET voltage is $\sim -1$ V and the RESET voltage is near 2.2 V. The ON/OFF current ratio can be over $10^3$ at $-1$ V. The retention time is more than $10^4$ s and the HRS/LRS resistance degrades little after $10^8$ read cycles, which indicates TPAPAM, served as hole-transport agent, greatly improves the stability of GO RRAM.

Although the high stability and low SET voltage are obtained in these RRAMs, the ON/OFF current ratio needs further improvement. Reference [116] proposed Pt/rGO–thionine(th)/Pt RRAM and the layered rGO–th film flakes can be obtained by filtering the rGO–th solution and transfer to other substrate. The rGO film decorated by thionine owns a large resistance, which can be as high as $7\times10^7$ Ω in the OFF state. These features guarantee a relative high ON/OFF ratio. For this device, the ratio can reach up to $5\times10^4$ with the read voltage 0.1 V, improving near 50 times compared to TPAPAM-GO based RRAM. The switching mechanism is different from the ordinary filament forming and rupturing. It depends on whether the conductive path built by linking thionine molecules and further reduced GO between two electrodes is connected or disconnected. Similar to the filament, this conductive path is to transport charge with little hindrance and its connection or disconnection is determined by the external voltage, making the device show the HRS and LRS resistance switching behavior. The SET voltage varies from 1.91 V to 3.93 V, while the RESET one from $-0.47$ V to $-1.04$ V, which indicates that the conductive path is hard to form and easy to break down, needing high SET voltage and low RESET voltage. Moreover, this device also owns fast switching speed ($< 5$ ns) and long retention time (over $10^5$ s). After 350 switching cycles, the resistances do not show obvious degradation, exhibiting good endurance and stability.

Other GO–polymer composites are also used as the switching layer to improve GO RRAM properties. GO–PI

based RRAM[117] can achieve multilevel resistive switching owing to the trapping effect in GO–PI film. GO–polypyrrole (PPy)[118] based RRAM realizes a high ON/OFF current ratio over $10^5$ with good stability and solves the problem of the low ON/OFF current ratio for ordinary GO RRAM issue well.

**(ii) Nanoparticle** GO-based memory decorated by nanoparticle, such as Au, can improve the memory switching property.[119,120] Reference [121] presented a gold nanoparticle decorated rGO RRAM (Al/Au Nps–rGO–PVA/Pt) with polyvinyl alcohol (PVA) matrix. The Au decorated rGO sheet is synthesized by using the mixture of $HAuCl_4$ solution (2.5 mM, 10 ml), GO flakes (20 mg), and aqueous PVA solution (1 wt.%, 50 ml). After 10 h stirring, a sodium borohydride solution (10 ml) is used to reduce the GO and $Au^{3+}$ to rGO and Au NP to obtain the Au NPs–rGO–PVA film. Because this device is fabricated on the PET substrate, it owns high flexibility, which is very suitable for flexible circuit application. The Au NP acts as the filament linker between rGO sheets and helps lower the SET voltage ($-0.44$ V) compared to the control rGO RRAM ($\sim -5.6$ V). For GO RRAM, the reduction and oxidation of GO under different voltage bias is the key to form or rupture conductive filament. The interfacial defects near Au NP can act as trapping sites and accelerate this process by the internal electrical field generated by these sites. Apart from that, the device owns a relatively high ON/OFF current ratio ($> 10^3$), larger than that of the control GO RRAM ($\sim 2.5 \times 10^2$). The relatively long retention time ($> 10^4$ s) shows the good endurance. But when the cycles are increased to some degree, the fluctuation of SET and RESET voltages becomes a little large.

Other kinds of nanoparticles, such as Ni,[122] are used to improve and change the RRAM behavior, showing the promising application in memory and neuromorphic field.

**(iii) 2D materials** 2D materials are similar to $\pi$-conjugated polymers, which are layered, have a plane-like structure, and own many excellent electrical and optical properties.[123–127] GO decorated by 2D materials can also improve the switching property for RRAM. Reference [128] used the $MoS_2$–GO composite as the active layer to fabricate GO RRAM. Because $MoS_2$ has larger conductivity than GO, the $MoS_2$ component in the $MoS_2$–GO film will increase the whole composite conductivity and facilitate oxygen migration in GO when the external voltage is applied. Therefore, low SET ($\sim -1.2$ V) and RESET($\sim 1.5$ V) voltages can be obtained. But the ON/OFF current ratio ($\sim 10^2$) is a bit small due to the low resistance in HRS.

## 4. Concluding remarks

In this review, we have shown 8 main merits and roles of graphene as the electrode for RRAM, multilevel switching, and improvement of RRAM with graphene as the sandwiched middle layer, and graphene-based GO/rGO RRAM. However, the graphene RRAMs are so diverse that the lists are not able to include all of them. Compared to ordinary RRAM, the low power consumption, higher density, transparency, SET voltage controllable, etc. properties of graphene RRAM and lower SET voltage, flexible, easy to fabricate, etc. properties of rGO/GO RRAM make them have strong competitive power in the memory field, even though many issues for graphene are currently existing, such as growth and pattern of graphene are hard to integrate to the standard silicon manufacturing process, and the ON/OFF current ratio of GO RRAM is not high enough. With the fabrication process technology improving, we believe these issues will be solved and graphene RRAM will exhibit great potential on memory and neuromorphic applications separately in the further scaled down, flexible, or transparent circuit.

## References


[1] Russo U, Ielmini D, Cagli C and Lacaita A L 2009 *IEEE Trans. Electron Devices* **56** 193
[2] Wong H-S P, Lee H Y, Yu S, Chen Y S, Wu Y, Chen P S, Lee B, Chen F T and Tsai M J 2012 *Proc. IEEE* **100** 1951
[3] Bersuker G, Gilmer D, Veksler D, Kirsch P, Vandelli L, Padovani A and Iglesias V 2011 *J. Appl. Phys.* **110** 124518
[4] Yu S, Guan X and Wong H S P 2011 *IEEE International Electron Devices Meeting*, December 5–7, 2011, Washington, D.C., USA, p. 17.3.1
[5] Hosoi Y, Tamai Y, Ohnishi T, Ishihara K, Shibuya T, Inoue Y, Yamazaki S, Nakano T, Ohnishi S and Awaya N 2006 *International Electron Devices Meeting*, December 11–13, 2006, San Francisco, USA, p. 1
[6] Ielmini D 2011 *IEEE Trans. Electron Devices* **58** 4309
[7] Wang L, Yang C H and Wen J 2015 *Electron. Mater. Lett.* **11** 505
[8] Meena J S, Sze S M, Chand U and Tseng T Y 2014 *Nanoscale Res. Lett.* **9** 1
[9] Choi B J, Torrezan A C, Norris K J, Miao F, Strachan J P, Zhang M X, Ohlberg D A, Kobayashi N P, Yang J J and Williams R S 2013 *Nano Lett.* **13** 3213
[10] Lee M J, Lee C B, Lee D, Lee S R, Chang M, Hur J H, Kim Y B, Kim C J, Seo D H and Seo S 2011 *Nat. Mater.* **10** 625
[11] Wei Z, Kanzawa Y, Arita K, Katoh Y, Kawai K, Muraoka S, Mitani S, Fujii S, Katayama K and Iijima M 2008 *IEEE International Electron Devices Meeting*, December 15–17, 2008, San Francisco, USA, p. 1
[12] Guan X, Yu S and Wong H S P 2012 *IEEE Trans. Electron Devices* **59** 1172
[13] Yu S, Guan X and Wong H S P 2012 *IEEE Trans. Electron Devices* **59** 1183
[14] Sheridan P, Kim K H, Gaba S, Chang T, Chen L and Lu W 2011 *Nanoscale* **3** 3833
[15] Celano U, Chen Y Y, Wouters D J, Groeseneken G, Jurczak M and Vandervorst W 2013 *Appl. Phys. Lett.* **102** 121602
[16] Chang W Y, Lai Y C, Wu T B, Wang S F, Chen F and Tsai M J 2008 *Appl. Phys. Lett.* **92** 2110
[17] Wu X, Zhou P, Li J, Chen L, Lv H, Lin Y and Tang T 2007 *Appl. Phys. Lett.* **90** 183507
[18] Jeong H Y, Kim Y I, Lee J Y and Choi S Y 2010 *Nanotechnology* **21** 115203
[19] Son J Y, Shin Y H, Kim H and Jang H M 2010 *ACS Nano* **4** 2655
[20] Zhang H, Liu L, Gao B, Qiu Y, Liu X, Lu J, Han R, Kang J and Yu B 2011 *Appl. Phys. Lett.* **98** 042105
[21] Wu Y, Yu S, Lee B and Wong P 2011 *J. Appl. Phys.* **110** 094104
[22] Wang Z, Zeng F, Yang J, Chen C, Yang Y and Pan F 2010 *Appl. Phys. Lett.* **97** 253301
[23] Chen Y C, Chen C, Chen C, Yu J, Wu S, Lung S, Liu R and Lu C Y 2003 *International Electron Devices Meeting*, December 8–10, 2003, Washington, D.C., USA, p. 37.4.1
[24] Novoselov K, Geim A K, Morozov S, Jiang D, Katsnelson M, Grigorieva I, Dubonos S and Firsov A 2005 *Nature* **438** 197
[25] Orlita M, Faugeras C, Plochocka P, Neugebauer P, Martinez G, Maude D K, Barra A L, Sprinkle M, Berger C and De Heer W A 2008 *Phys. Rev. Lett.* **101** 267601
[26] Peres N, Guinea F and Neto A C 2006 *Phys. Rev. B* **73** 125411

[27] Nair R R, Blake P, Grigorenko A N, Novoselov K S, Booth T J, Stauber T, Peres N M and Geim A K 2008 *Science* **320** 1308
[28] Lee C, Wei X, Kysar J W and Hone J 2008 *Science* **321** 385
[29] Sun Z S, Zhang L and Gao F 2016 *Chin. Phys. B* **25** 0108701
[30] Jiang R, Wu Z R, Han Z Y and Jung H S 2016 *Chin. Phys. B.* **25** 0106803
[31] Lin Y M, Jenkins K A, Valdes-Garcia A, Small J P, Farmer D B and Avouris P 2008 *Nano Lett.* **9** 422
[32] Feng T, Xie D, Lin Y, Zang Y, Ren T, Song R, Zhao H, Tian H, Li X and Zhu H 2011 *Appl. Phys. Lett.* **99** 233505
[33] Tian H, Xie D, Yang Y, Ren T L, Wang Y F, Zhou C J, Peng P G, Wang L G and Liu L T 2012 *Nanoscale* **4** 2272
[34] Schedin F, Geim A, Morozov S, Hill E, Blake P, Katsnelson M and Novoselov K 2007 *2007 Nat. Mater.* **6** 652
[35] Liu N, Tian H, Schwartz G, Tok J B H, Ren T L and Bao Z 2014 *Nano Lett.* **14** 3702
[36] Li X, Cai W, An J, Kim S, Nah J, Yang D, Piner R, Velamakanni A, Jung I and Tutuc E 2009 *Science* **324** 1312
[37] Losurdo M, Giangregorio M M, Capezzuto P and Bruno G 2011 *PCCP* **13** 20836
[38] Hirata M, Gotou T and Ohba M 2005 *Carbon* **43** 503
[39] Strong V, Dubin S, El-Kady M F, Lech A, Wang Y, Weiller B H and Kaner R B 2012 *ACS Nano* **6** 139
[40] El-Kady M F, Strong V, Dubin S and Kaner R B 2012 *Science* **335** 1326
[41] Gómez-Navarro C, Weitz R T, Bittner A M, Scolari M, Mews A, Burghard M and Kern K 2007 *Nano Lett.* **7** 3499
[42] Eda G, Fanchini G and Chhowalla M 2008 *Nat. Nanotechnol.* **3** 270
[43] Tian H, Shu Y, Wang X F, Mohammad M A, Bie Z, Xie Q Y, Li C, Mi W T, Yang Y and Ren T L 2015 *Sci. Rep.* **5**
[44] Tian H, Xie D, Yang Y, Ren T L, Zhang G, Wang Y F, Zhou C J, Peng P G, Wang L G and Liu L T 2012 *Sci. Rep.* **2** 523
[45] Tian H,Yang Y, Xie D, Ren T L, Shu Y, Zhou C J, Tao L Q and Liu L T 2013 *IEEE 26th International Conference*, September 4–6 2013, Erlangen, Germany, p. 709
[46] Tian H, Yang Y, Xie D, Ge J and Ren T L 2013 *RSC Adv.* **3** 17672
[47] Tian H, Shu Y, Cui Y L, Mi W T, Yang Y, Xie D and Ren T L 2014 *Nanoscale* **6** 699
[48] Wang X, Tian H, Mohammad M A, Li C, Wu C, Yang Y and Ren T L 2015 *Nat. Commun.* **6** 7767
[49] Xia F, Perebeinos V, Lin Y M, Wu Y and Avouris P 2011 *Nat. Nanotechnol.* **6** 179
[50] Chen H Y, Tian H, Gao B, Yu S, Liang J, Kang J, Zhang Y, Ren T L and Wong H S P 2012 *IEEE International Electron Devices Meeting*, December 10–13, 2012, San Francisco, USA, p. 20.5.1
[51] Tian H, Chen H Y, Gao B, Yu S, Liang J, Yang Y, Xie D, Kang J, Ren T L and Zhang Y 2013 *Nano Lett.* **13** 651
[52] Ferrari A C 2007 *Solid State Commun.* **143** 47
[53] Ryu S, Liu L, Berciaud S, Yu Y J, Liu H, Kim P, Flynn G W and Brus L E 2010 *Nano Lett.* **10** 4944
[54] Jeon H, Park J, Jang W, Kim H, Ahn S, Jeon K J, Seo H and Jeon H 2014 *Carbon* **75** 209
[55] Chen H Y, Yu S, Gao B, Liu R, Jiang Z, Deng Y, Chen B, Kang J and Wong H P 2013 *Nanotechnology* **24** 465201
[56] Sohn J, Lee S, Jiang Z, Chen H Y and Wong H S P 2014 *IEEE International Electron Devices Meeting*, December 15–17, 2014, San Francisco, USA, p. 5.3.1
[57] Deng Y, Chen H Y, Gao B, Yu S, Wu S C, Zhao L, Chen B, Jiang Z, Liu X and Hou T H 2013 *IEEE International Electron Devices Meeting*, December 9–11, 2013, Washington, D.C., USA, p. 25.7.1
[58] Cheng H, Chen S, Yu P, Duan X, Xie B and Tian, J 2013 *Appl. Phys. Lett.* **103** 203112
[59] Bae S, Kim H, Lee Y, Xu X, Park J S, Zheng Y, Balakrishnan J, Lei T, Kim H R and Song Y I 2010 *Nat. Nanotechnol.* **5** 574
[60] Yang P K, Chang W Y, Teng P Y, Jeng S F, Lin S J, Chiu P W and He J H 2013 *Proc. IEEE* **101** 1732
[61] Sato Y, Takai K and Enoki T 2011 *Nano Lett.* **11** 3468
[62] Chang W, Chu J and Wang S 2012 *Appl. Phys. Lett.* **101** 012102
[63] Zhao H, Tu H, Wei F, Xiong Y, Zhang X and Du J 2013 *RRL-Rapid Res. Lett.* **7** 1005
[64] Cao X, Li X, Gao X, Yu W, Liu X, Zhang Y, Chen L and Cheng X 2009 *J. Appl. Phys.* **106** 073723
[65] Zhao H, Tu H, Wei F and Du J 2014 *IEEE Trans. Electron Devices* **61** 1388
[66] Thomas G 1997 *Nature* **389** 907
[67] Lu H, Sun K, Zhang K, Wang F, Miao Y and Wang B 2014 *ECS Trans.* **60** 545
[68] Seo S, Lee M, Kim D, Ahn S, Park B H, Kim Y, Yoo I, Byun I, Hwang I and Kim S 2005 *Appl. Phys. Lett.* **87** 263507
[69] Son J Y, Shin Y H, Kim H and Jang H M 2010 *ACS Nano* **4** 2655
[70] Nagaraj B, Wu T, Ogale S, Venkatesan T and Ramesh R 2002 *J. Electroceram.* **8** 233
[71] Kim W H, Park C S and Son J Y 2014 *Carbon* **79** 388
[72] Li C X, Deng X Q and Sun L 2016 *Acta Phys. Sin.* **65** 068503 (in Chinese)
[73] McCann E 2006 *Phys. Rev. B* **74** 161403
[74] Ohta T, Bostwick A, Seyller T, Horn K and Rotenberg E 2006 *Science* **313** 951
[75] Castro E V, Novoselov K, Morozov S, Peres N, Dos Santos J L, Nilsson J, Guinea F, Geim A and Neto A C 2007 *Phys. Rev. Lett.* **99** 216802
[76] McCann E and Koshino M 2013 *Rep. Prog. Phys.* **76** 056503
[77] Tian H, Zhao H, Wang X F, Xie Q Y, Chen H Y, Mohammad M A, Li C, Mi W T, Bie Z, Chao H Y, Yang Y, Wong H P, Chiu P W and Ren T L 2015 *Adv. Mater.* **27** 7767
[78] Rozenberg M, Inoue I and Sanchez M 2004 *Phys. Rev. Lett.* **92** 178302
[79] Waser R and Aono M 2007 *Nat. Mater.* **6** 833
[80] Lee S R, Kim Y B, Chang M, Kim K M, Lee C B, Hur J H, Park G S, Lee D, Lee M J and Kim C J 2012 *Symposium on VLSI Technology*, June 12–14, 2012, Honolulu, USA, p. 71
[81] Wu M C, Lin Y W, Jang W Y, Lin C H and Tseng T Y 2011 *IEEE Electron Device Lett.* **32** 1026
[82] He C, Shi Z, Zhang L, Yang W, Yang R, Shi D and Zhang G 2012 *ACS Nano* **6** 4214
[83] Liao A D, Wu J Z, Wang X, Tahy K, Jena D, Dai H and Pop E 2011 *Phys. Rev. Lett.* **106** 256801
[84] Yu S, Guan X and Wong H S P 2011 *Appl. Phys. Lett.* **99** 063507
[85] Valanarasu S, Kathalingam A, Senthilkumar V, Kannan V and Rhee J 2012 *Electron. Mater. Lett.* **8** 649
[86] Khurana G, Misra P and Katiyar R S 2014 *Carbon* **76** 341
[87] Kane B 2010 *Phys. Rev. B* **82** 115441
[88] Yang R, Zhu C, Meng J, Huo Z, Cheng M, Liu D, Yang W, Shi D, Liu M and Zhang G 2013 *Sci. Rep.* **3** 2126
[89] Rose A 1955 *Phys. Rev.* **97** 1538
[90] Tian H, Chen H Y, Ren T L, Li C, Xue Q T, Mohammad M A, Wu C, Yang Y and Wong H S P 2014 *Nano Lett.* **14** 3214
[91] Fang Z, Yu H, Li X, Singh N, Lo G and Kwong D 2011 *IEEE Electron Device Lett.* **32** 566
[92] Miao F, Strachan J P, Yang J J, Zhang M X, Goldfarb I, Torrezan A C, Eschbach P, Kelley R D, Medeiros-Ribeiro G and Williams R S 2011 *Adv. Mater.* **23** 5633
[93] Panin G N, Kapitanova O O, Lee S W, Baranov A N and Kang T W 2011 *Jpn. J. Appl. Phys.* **50** 070110
[94] Jilani S M, Gamot T D, Banerji P and Chakraborty S 2013 *Carbon* **64** 187
[95] Yuan F, Ye Y R, Wang J C, Zhang Z, Pan L, Xu J and Lai C S 2013 *IEEE 5th International Nanoelectronics Conference*, January 2–4 2013, Singapore, p. 288
[96] Kapitanova O, Panin G, Kononenko O, Baranov A and Kang T 2014 *J. Korean Phys. Soc.* **64** 1399
[97] Yi M D, Guo J L, Hu B, Xia X H, Fan Q L, Xie L H and Huang W 2015 *Chin. Phys. Lett.* **32** 077201
[98] Eda G, Mattevi C, Yamaguchi H, Kim H and Chhowalla M 2009 *J. Phys. Chem. C* **113** 15768
[99] Ekiz O O, Urel M, Guner H, Mizrak A K and D'ana A 2011 *ACS Nano* **5** 2475
[100] Lim E W, Ahmadi M T and Ismail R 2016 *J. Comput. Electron.* **15** 602
[101] Herrmann M and Schenk A 1995 *J. Appl. Phys.* **77** 4522
[102] Bocquet M, Deleruyelle D, Muller C and Portal J M 2011 *Appl. Phys. Lett.* **98** 263507
[103] Grierson D S, Sumant A, Konicek A, Friedmann T, Sullivan J and Carpick R W 2010 *J. Appl. Phys.* **107** 033523
[104] Laidler K J 1984 *J. Chem. Educ.* **61** 494
[105] Lampert M A 1956 *Phys. Rev.* **103** 1648
[106] Zhuang X D, Chen Y, Liu G, Li P P, Zhu C X, Kang E T, Noeh K G, Zhang B, Zhu J H and Li Y X 2010 *Adv. Mater.* **22** 1731

[107] He C, Zhuge F, Zhou X, Li M, Zhou G, Liu Y, Wang J, Chen B, Su W and Liu Z 2009 *Appl. Phys. Lett.* **95** 232101
[108] Jeong H Y, Kim J Y, Kim J W, Hwang J O, Kim J E, Lee J Y, Yoon T H, Cho B J, Kim S O and Ruoff R S 2010 *Nano Lett.* **10** 4381
[109] Lee D H, Kim J E, Han T H, Hwang J W, Jeon S, Choi S Y, Hong S H, Lee W J, Ruoff R S and Kim S O 2010 *Adv. Mater.* **22** 1247
[110] Kim S K, Kim J Y, Choi S Y, Lee J Y and Jeong H Y 2015 *Adv. Funct. Mater.* **25** 6710
[111] Zhuge F, Hu B, He C, Zhou X, Liu Z and Li R W 2011 *Carbon* **49** 3796
[112] Wang Z, Tjoa V, Wu L, Liu W, Fang Z, Tran X, Wei J, Zhu W and Yu H 2012 *J. Electrochem. Soc.* **159** K177
[113] Kim I, Siddik M, Shin J, Biju K P, Jung S and Hwang H 2011 *Appl. Phys. Lett.* **99** 042101
[114] Li S L, Liao Z, Li J, Gang J and Zheng D 2009 *J. Phys. D: Appl. Phys.* **42** 045411
[115] Nian Y, Strozier J, Wu N, Chen X and Ignatiev A 2007 *Phys. Rev. Lett.* **98** 146403
[116] Hu B, Quhe R, Chen C, Zhuge F, Zhu X, Peng S, Chen X, Pan L, Wu Y and Zheng W 2012 *J. Mater. Chem.* **22** 16422
[117] Wu C, Li F, Zhang Y, Guo T and Chen T 2011 *Appl. Phys. Lett.* **99** 042108
[118] Li Y, Ni X and Ding S 2015 *J. Mater. Sci. Mater. Electron.* **26** 9001
[119] Myung S, Park J, Lee H, Kim K S and Hong S 2010 *Adv. Mater.* **22** 2045
[120] Wang W and Ma D G 2010 *Chin. Phys. Lett.* **27** 018503
[121] Midya A, Gogurla N and Ray S K 2015 *Curr. Appl Phys.* **15** 706
[122] Pinto S, Krishna R, Dias C, Pimentel G, Oliveira G, Teixeira J, Aguiar P, Titus E, Gracio J and Ventura J 2012 *Appl. Phys. Lett.* **101** 063104
[123] Radisavljevic B, Radenovic A, Brivio J, Giacometti i V and Kis A. 2011 *Nat. Nanotechnol.* **6** 147
[124] Shao P Z, Zhao H M, Cao H W, Wang X F, Pang Y, Li Y X, Deng N Q, Zhang J, Zhang G Y, Yang Y, Zhang S and Ren T L 2016 *Appl. Phys. Lett.* **108** 203105
[125] Cao H W, Zhao H M, Xin X, Shao P Z, Qi H Y, Jian M Q, Zhang Y Y, Yang Y and Ren T L 2016 *Mod. Phys. Lett. B* **30** 1650267
[126] Podzorov V, Gershenson M, Kloc C, Zeis R and Bucher E 2004 *Appl. Phys. Lett.* **84** 3301
[127] Liu W, Kang J, Sarkar D, Khatami Y, Jena D and Banerjee K 2013 *Nano Lett.* **13** 1983
[128] Yin Z, Zeng Z, Liu J, He Q, Chen P and Zhang H 2013 *Small* **9** 727